applied sciences

MDPI

Communication

Experimental and 2-Step Finite Element Analysis of Cyclic Fatigue Resistance of Conventional and Heat-Treated Rotary Endodontic Nickel-Titanium Instruments

Philip Yuan-Ho Chien [1], Boyang Wan [2], Laurence James Walsh [1] and Ove Andreas Peters [1,*]

[1] School of Dentistry, The University of Queensland, Brisbane, QLD 4006, Australia
[2] School of Aerospace, Mechanical and Mechatronic Engineering, The University of Sydney, Sydney, NSW 2006, Australia
* Correspondence: o.peters@uq.edu.au

Abstract: Background: To evaluate the cyclic fatigue resistance of rotary endodontic nickel-titanium instruments using both experimental and finite element methods. Methodology: Four different proprietary rotary endodontic instruments (PTG, PTU, VB, and TRN) were subjected to cyclic fatigue tests through a custom-built fixture (n = 30 for each group) and tested until failure according to the manufacturer's recommended settings, and the number of cycles to failure (NCF) was measured. Separated fragments were measured to determine the location of the fracture event. Finite element modeling replicated this experiment in silico via a two-step method, modeling the dynamic motion via an initial insertion step, then followed by rotation. Results: TRN showed the highest NCF (2027.94 ± 452.50) with the lowest values for strain (4.49% ± 0.23%) and fragment lengths (3.26 mm ± 0.47 mm), whereas PTU showed the lowest NCF (600.90 ± 80.86) and highest values for strain (6.29% ± 0.47%) and fragment lengths (5.36 mm ± 0.79 mm). All instruments showed an increase in von Mises and maximum principal stress during the insertion step but showed no changes to the maximum stress values during the rotational step. Conclusions: The finite element analysis approach used provided useful insights into the stress evolution and stress distribution of instruments during cyclic fatigue but lacked the ability with existing inputs to predict failure from cyclic fatigue.

Keywords: nitinol; endodontics; root canal therapy; ProTaper; cyclic fatigue; mechanical stress; finite element analysis; von Mises stress; dentistry

Citation: Chien, P.Y.-H.; Wan, B.; Walsh, L.J.; Peters, O.A. Experimental and 2-Step Finite Element Analysis of Cyclic Fatigue Resistance of Conventional and Heat-Treated Rotary Endodontic Nickel-Titanium Instruments. *Appl. Sci.* **2023**, *13*, 2080. https://doi.org/10.3390/app13042080

Academic Editor: Andrea Scribante

Received: 26 January 2023
Revised: 2 February 2023
Accepted: 3 February 2023
Published: 6 February 2023

1. Introduction

Cyclic fatigue of nickel-titanium (NiTi) endodontic instruments is a phenomenon caused by crack propagation from repeated tensile-compressive stresses and has been studied as early as 1997 [1,2]. Pruett et al. posited that static bending tests of engine-driven instruments were unsuitable for the assessment of their dynamic properties and designed a model in which the instrument could rotate freely [2]. Between 2014 and 2018, an electronic literature search strategy identified as many as 68 studies on cyclic fatigue that were published in the Journal of Endodontics and the International Endodontic Journal [3]. Despite the large number of studies on this specific phenomenon, many investigations were previously examined for their lack of standardization and questioned on usefulness for informing clinical practice [4].

Recent studies have approached the experimental investigation of the mechanical behavior of instruments using novel methods to the traditional static and dynamic fatigue tests, such as examining the effect of wire diameter in relationship to cyclic and torsional fatigue [5], or the impact of metallurgical characteristics on torsional resistance [6]. In tandem with the growing interest in experimental investigations of fatigue and torsional resistance in endodontic NiTi instruments, the number of published finite element analysis (FEA)

studies on the mechanical behavior of rotary endodontic instruments has also increased significantly in the last decade [7,8].

The finite element method (FEM) is particularly useful in observing stress behaviors that are not measurable in physical experiments. In short, FEM begins by defining the problem, including the relevant geometry, properties, loads and boundary conditions. As real structures and components are generally very complex, reduction and compromise are normally required to create a manageable geometry [9]. The geometrical model is "meshed" by discretizing the body into an optimal number of arbitrary 2D or 3D elements ("finite elements"), resulting in matrix equations relating the input at specified points in the elements (nodes) to the output at these same points [9,10]. The sum of these matrix equations from the nodes results in a global matrix equation and can be used to solve equations over larger regions [10]. Once solved, the results are then interpreted and validated.

With the advent of improved computer processing power and finite element software development, complex matrix equations that were historically solved manually can now be calculated with increased accuracy and efficiency. Particularly in the case of complex geometrical structures, such as a rotary endodontic instrument, using finite element models is appropriate. The task of the user is to ensure the problem is well defined, with a geometrical approximation that accurately reflects the true geometry of the instrument.

Despite the recent surge in publications of FEA of NiTi instruments, cyclic fatigue is currently not well studied when compared to static bending and torsion [8]. To date, only one study has reproduced the number of cycles to failure (NCF) data on FEA [11]. Given this background, the present study aims to compare experimental cyclic fatigue data from a proposed standardized fatigue device with a two-step routine in FEA, in which both the instruments and fatigue device are modeled closely in terms of geometry and boundary conditions.

2. Materials and Methods

Four different proprietary rotary endodontic instruments (PTG, PTU, VB, and TRN) with varying NiTi alloy types were used (Table 1). Instruments were subjected to cyclic fatigue testing through a custom-built cyclic fatigue fixture proposed as an additional test for the ISO 3630-1 standard, the specifications of which are found in previously published works [7,12]. The instruments (n = 30) were run until failure according to the manufacturer's recommended settings in the R5 fixture, which has a radius of 5 mm with a maximum angle of curvature of 75° (Figure 1).

A high-resolution video (30 frames per second) was recorded for each run. The number of cycles to failure (NCF) was determined using open-source video-analysis software (Kinovea 0.9.3, open-source software). The separated fragments were retrieved and measured with a micrometer to determine the location of the fracture, which was expressed as a distance from the tip of the instrument. NCF and the location of the fracture were used as dependent variables, and the strain (ε) was calculated using Equation (1) to ensure the tests were valid under an 8% strain.

$$\varepsilon_T = \frac{d}{(2r)} \quad (1)$$

Table 1. List of rotary NiTi endodontic instruments selected, with the corresponding wire specimen that matches the metallurgical properties.

NiTi Wire Type	Corresponding NiTi Instrument	Size	Rotations per Minute (rpm)	Torque (Ncm)
Stock	ProTaper Universal™ F2, 25 mm (PTU)	25/06v	250	2.0
Gold	ProTaper Gold™ F2, 25 mm (PTG)	25/06v	300	3.1
Blue	Vortex Blue™, 25 mm (VB)	25/06v	500	2.8
Superflex	TruNatomyTM Prime, 25 mm (TRN)	26/04v	500	1.5

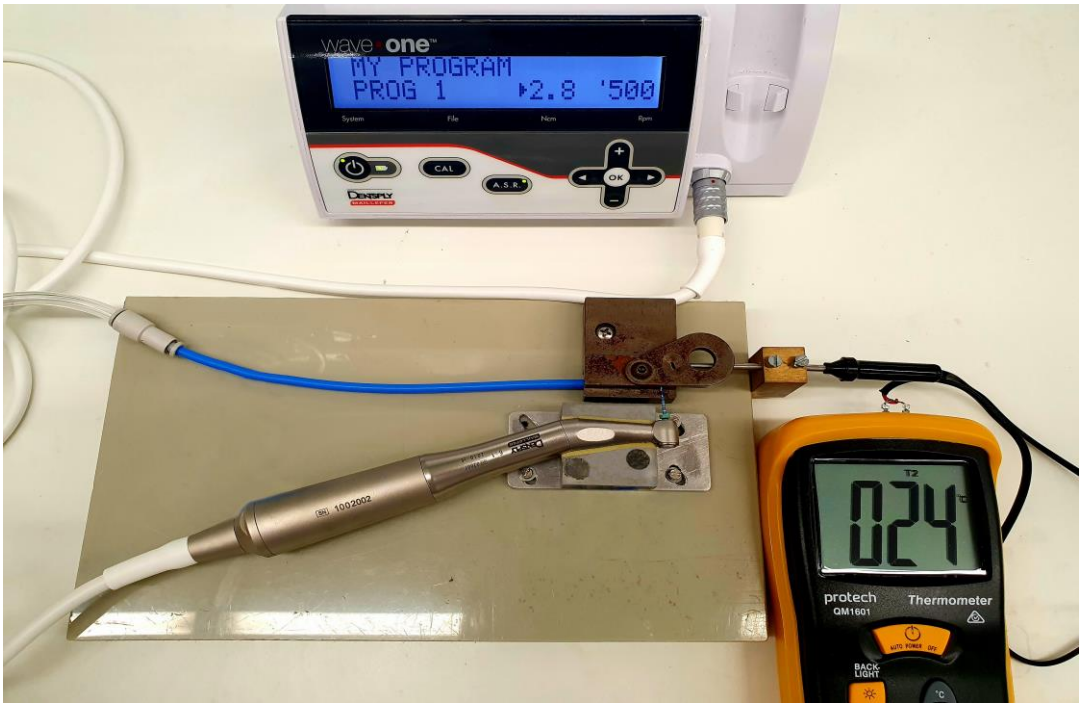

Figure 1. VB instrument set up with a cyclic fatigue rig with a thermocouple for tracking the temperature.

Micro-CT scans (μCT 40, Scanco Medical, Brüttisellen, Switzerland) of the PTU, VB, and TRN instruments were taken at 5.8 μm resolution, which generated three volume sets of DICOM data. As the PTU and PTG instruments have identical geometries, only a scan of the PTU instrument was required.

Using specialized imaging software (InVesalius 3.1, CTI, Sao Paolo, Brazil), the DICOM data were processed into a 3D model in the form of a Standard Tessellation Language (.STL) format. The instruments were also viewed under scanning electron microscopy (SEM) at 800× magnification as a confirmatory step for the cross-sectional geometry for PTU/PTG, VB, and TRN. The models were refined and repaired using SolidWorks 2016 (Dassault Systèmes SE, Vélizy-Villacoublay, France), and exported to ABAQUS 2016 software (Dassault Systèmes SE).

FEA was performed in ABAQUS/Explicit because of its capability of solving nonlinear behavior. The FE models were meshed using the solid continuum brick element (type: C3D4): PTU had 18,558 elements with 13,572 degrees of freedom (DOF), VB had 18,885 elements with 13,029 DOF, and TRN had 22,193 elements with 16,482 DOF. The .STL model of the R5 fatigue rig was supplied by Dentsply (Dentsply Maillefer Ballaigues, Switzerland).

The in-house measured elastic moduli and transformation stress values from microtensile tests in a study conducted by Chien et al., 2022, were implemented in ABAQUS through a user-defined material (VUMAT, ABQ_SUPER_ELASTIC_N3D) [13]. Material constants not determined from the experimental results in Chien et al., 2022, were extracted from the previous publication of Martins et al., 2022 [14]. The full list of material constants used is shown in Table 2.

Table 2. Material constants used for UMAT inputs for the subroutine module "ABQ_SUPER_ELASTIC_N3D".

Symbol	Parameter	PTU	PTG	VB	TRN
E_A	Austenite elasticity (MPa)	28,248	30,573	28,672	26,580
ν_A	Austenite Poisson's ration	0.33	0.33	0.33	0.33
E_M	Martensite elasticity (MPa)	20,146	21,254	20,900	21,029
ν_M	Martensite Poisson's ration	0.33	0.33	0.33	0.33
ε_L	Transformation strain	0.0445	0.0377	0.0385	0.0356
$(\delta\sigma/\delta T)_L$	$\delta\sigma/\delta T$ Loading	6.7	6.7	6.7	6.7
σ_{SL}	Start of transformation loading (MPa)	422	341	296	266
σ_{EL}	End of transformation loading (MPa)	481	424	351	366
T_0	Reference temperature (°C)	25	25	25	25
$(\delta\sigma/\delta T)_U$	$\delta\sigma/\delta T$ Unloading	6.7	6.7	6.7	6.7
σ_{SU}	Start of transformation unloading (MPa)	161	161	161	161
σ_{EU}	End of transformation unloading (MPa)	118	118	118	118
σ_{SCL}	Start of transformation stress in compression (MPa)	28,248	30,573	28,672	26,580

A two-step method for modeling the dynamic motion of the instruments was prescribed in FEA, as described below, and in Figure 2.

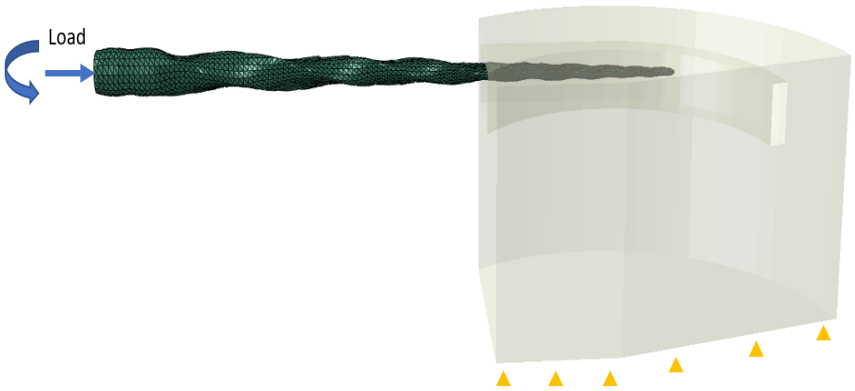

Figure 2. Loading and boundary conditions are applied in a two-step process for instrument models. Blue arrows show the loadings on the bottom surface of the instrument. The yellow triangles show the fixed support on the bottom surface of the rig.

Step-1: To mimic the insertion process, the displacement-driven load was applied on the bottom surface of the instrument to push the instrument into the fatigue rig, until 1 mm of the tip extruded from the fatigue rig. The bottom surface was kinematically constrained.

Step-2: To mimic the rotation of the instrument, a radian-driven input load was applied to the bottom surface of the instrument until the completion of the first rotation.

Using the ODB field output function in ABAQUS, the maximum von Mises stress and maximum principal stress values were tracked and plotted every over 20 increments (every 0.05 s) in step 1, by selecting the element (under the "Element Nodal" option in the field output) that expressed the highest peak values at the end of the insertion step, excluding any stress singularities. The changes in the stress values were recorded during the rotation in step 2. The location of the overall maximum von Mises stress and principal stress values were also recorded using the "Query" function to determine the distance from the tip of the instrument, and the location was compared to the experimental fragment length.

3. Results

All experimental runs showed a strain value greater than 2% and less than 8%, which are the strain limits that the proposed ISO-3630 standard considers valid [7]. Table 3 details the NCF, strain, and fragment length for the four selected instruments when tested at their manufacturer's recommended settings. TRN showed the highest NCF with the lowest values for strain and fragment lengths, whereas PTU showed the lowest NCF and the highest values for strain and fragment lengths.

Table 3. NCF, strain, and fragment data from cyclic fatigue testing for PTU, PTG, VB, and TRN.

Instrument	NCF (Dimensionless)	Strain (%)	Fragment (mm)
ProTaper Universal (PTU)	600.90 ± 80.86	6.29 ± 0.47	5.36 ± 0.79
ProTaper Gold (PTG)	1944.64 ± 189.86	5.98 ± 1.11	4.92 ± 1.80
Vortex Blue (VB)	1882.18 ± 353.35	4.66 ± 0.28	3.59 ± 0.47
TruNatomy (TRN)	2027.94 ± 452.50	4.49 ± 0.23	3.26 ± 0.47

Three-dimensional modeling of the instruments showed three distinct geometries, as seen in Figure 3.

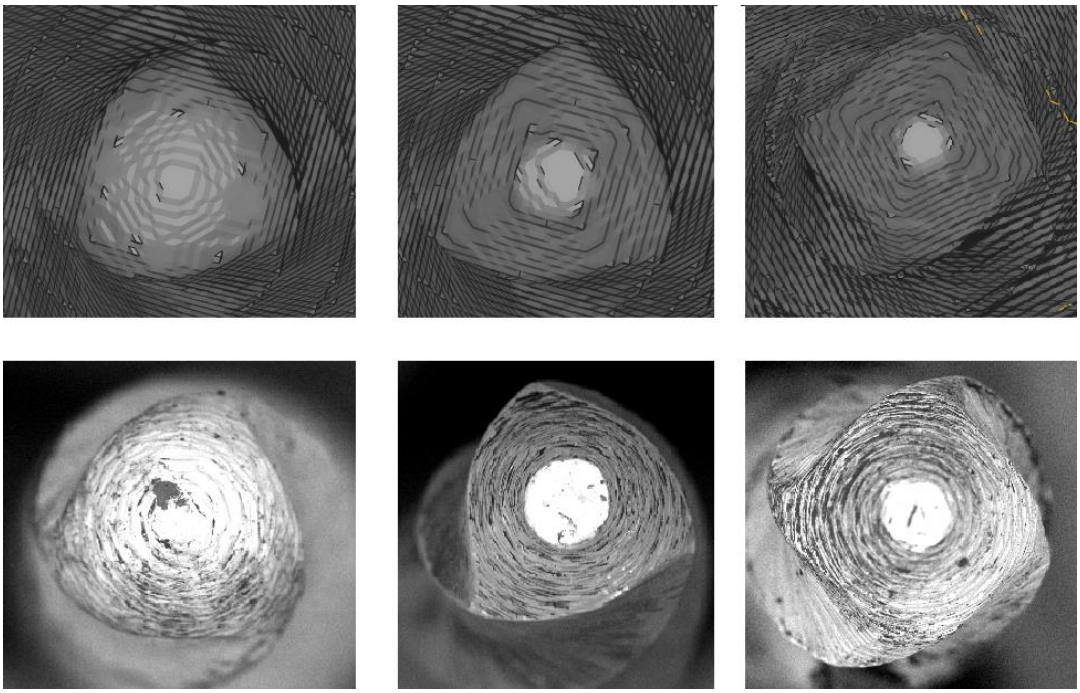

Figure 3. Top images showing geometries of the instrument tip for PTU/PTG, VB, and TRN (left to right) from .STL 3D models, viewed in Materialise MiniMagics 23.5 (Materialise, Leuven, Belgium). Bottom images show SEM microscopy at 800× magnification of the corresponding instrument tips.

PTU, PTG, and VB showed a cross-section that was convex triangular, whereas TRN was presented as an off-centered parallelogram cross-sectional design [15].

The overall geometry of the working portion of the instruments was also modeled, with only a small portion of the shaft (Figure 4). A mesh of the fatigue rig was also successfully obtained after adjustments in the SolidWorks software (Figure 4).

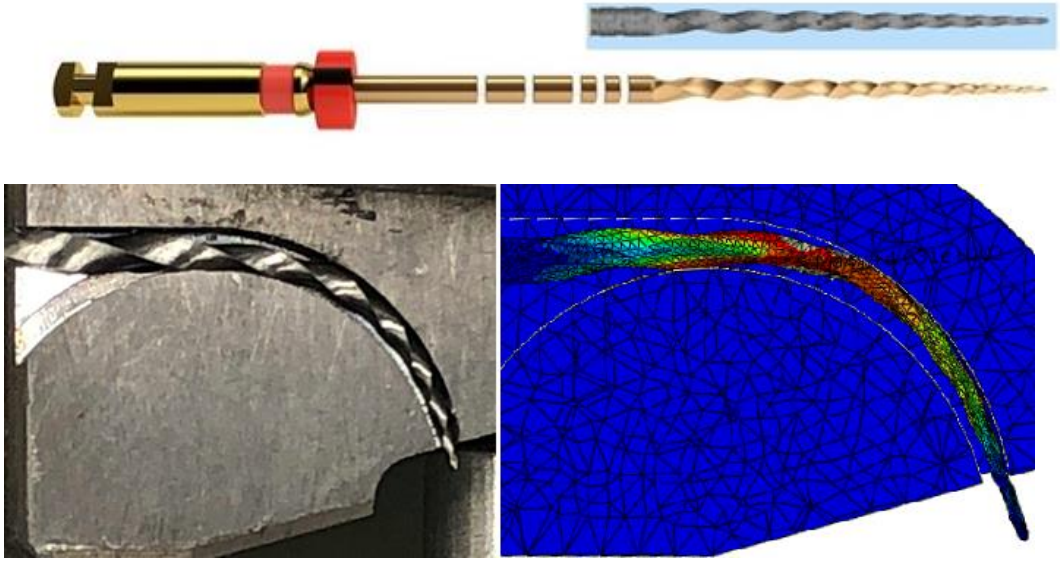

Figure 4. (**Top**): PTG F2 instrument with its .STL counterpart, viewed from Materialise MiniMagics 23.5. (**Bottom**): Comparison of VB instrument under light microscopy (**left**) vs. FE model (**right**).

All four simulations for PTU, PTG, VB, and TRN were completed successfully until the end of the step at 1 s. A plot for both the maximum von Mises stress and the maximum principal stress was reported for the entire insertion step of the simulation, but those values differed minimally (Figures 5A–D and 6). All plotted values remained below the ultimate tensile strength of the respective NiTi constituents. In general, there was an initial linear increase in von Mises stress in the first 0.2 s of insertion. PTG, VB, and TRN showed plateaus in stress values during 0.35–0.55 s, 0.55–0.85 s, and 0.30–0.60 s, respectively, whereas PTU did not exhibit this behavior.

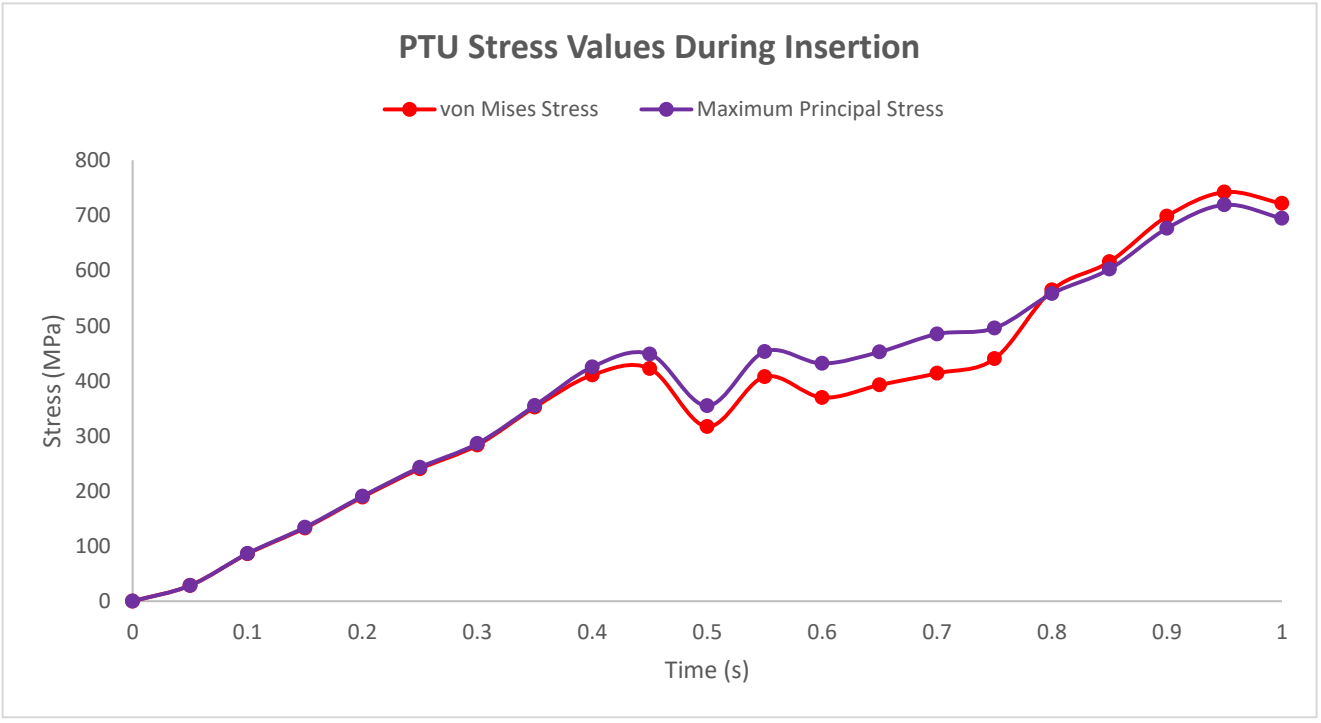

(**A**)

Figure 5. *Cont.*

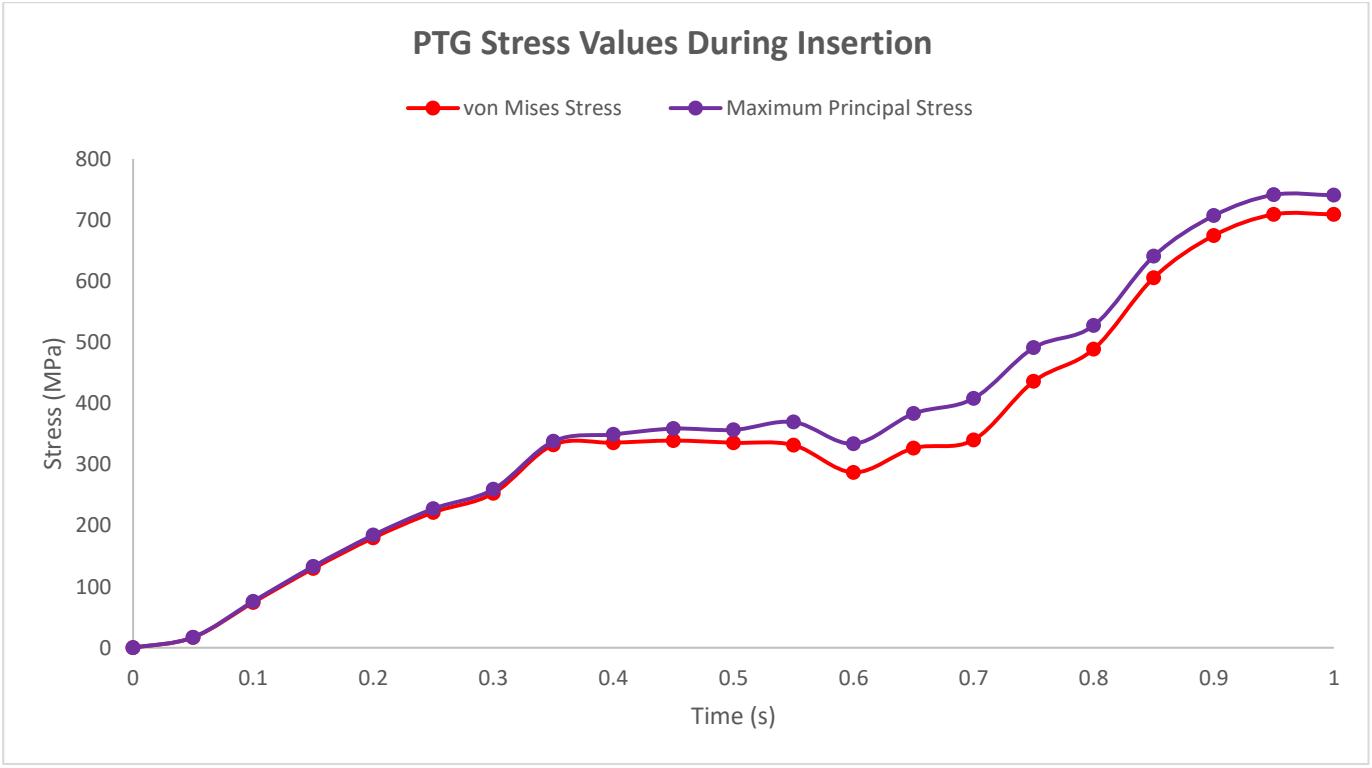

(**B**)

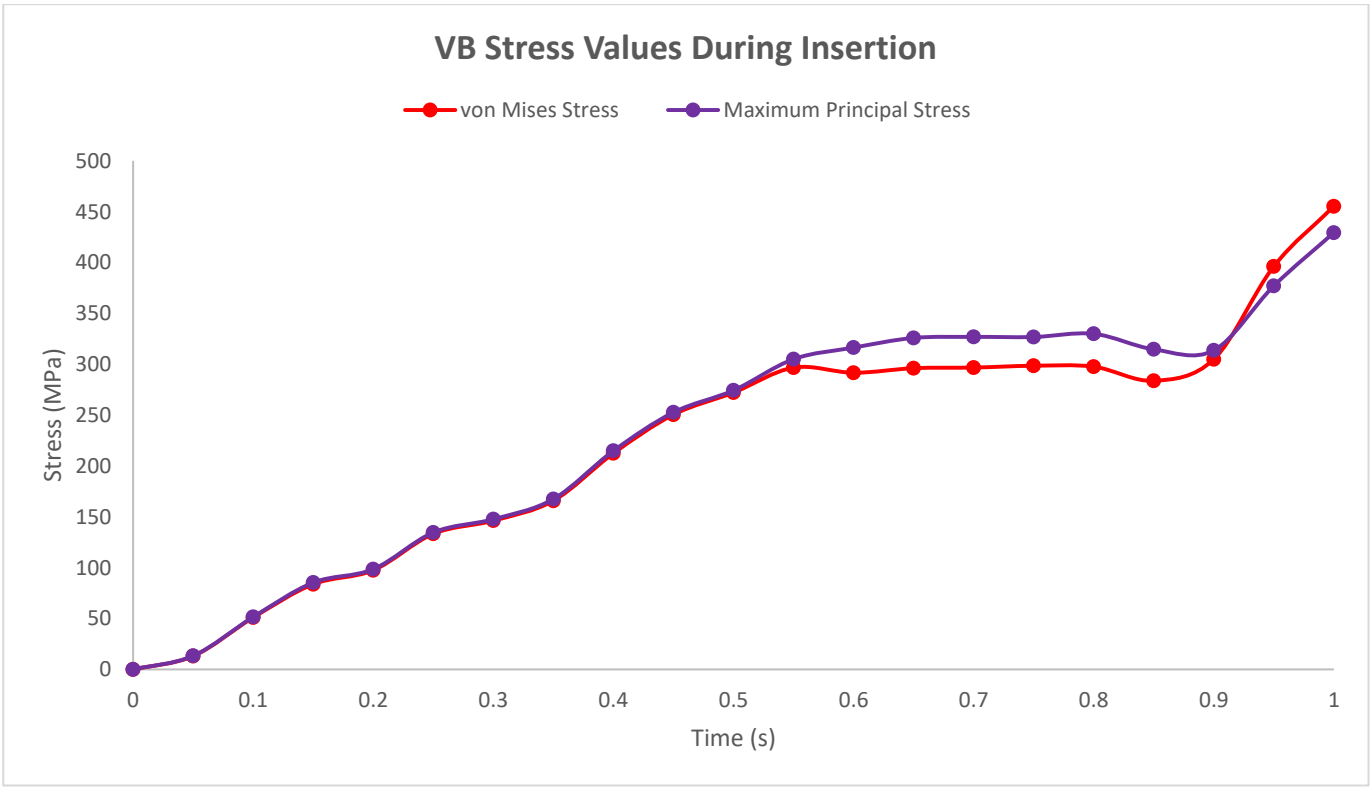

(**C**)

Figure 5. *Cont*.

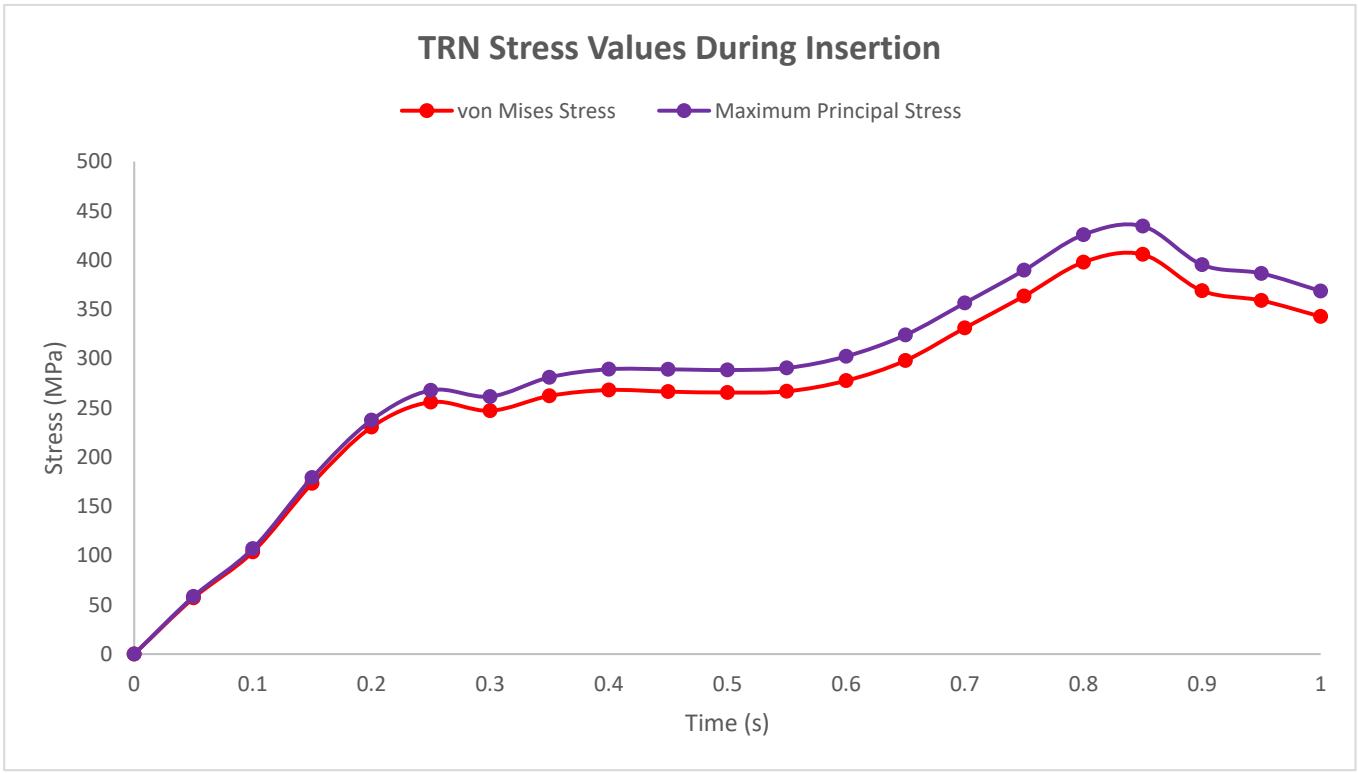

(**D**)

Figure 5. (**A**) PTU: Comparison of von Mises and maximum principal stress values during insertion. (**B**) PTG: Comparison of von Mises and maximum principal stress values during insertion. (**C**) VB: Comparison of von Mises and maximum principal stress values during insertion. (**D**) TRN: Comparison of von Mises and maximum principal stress values during insertion.

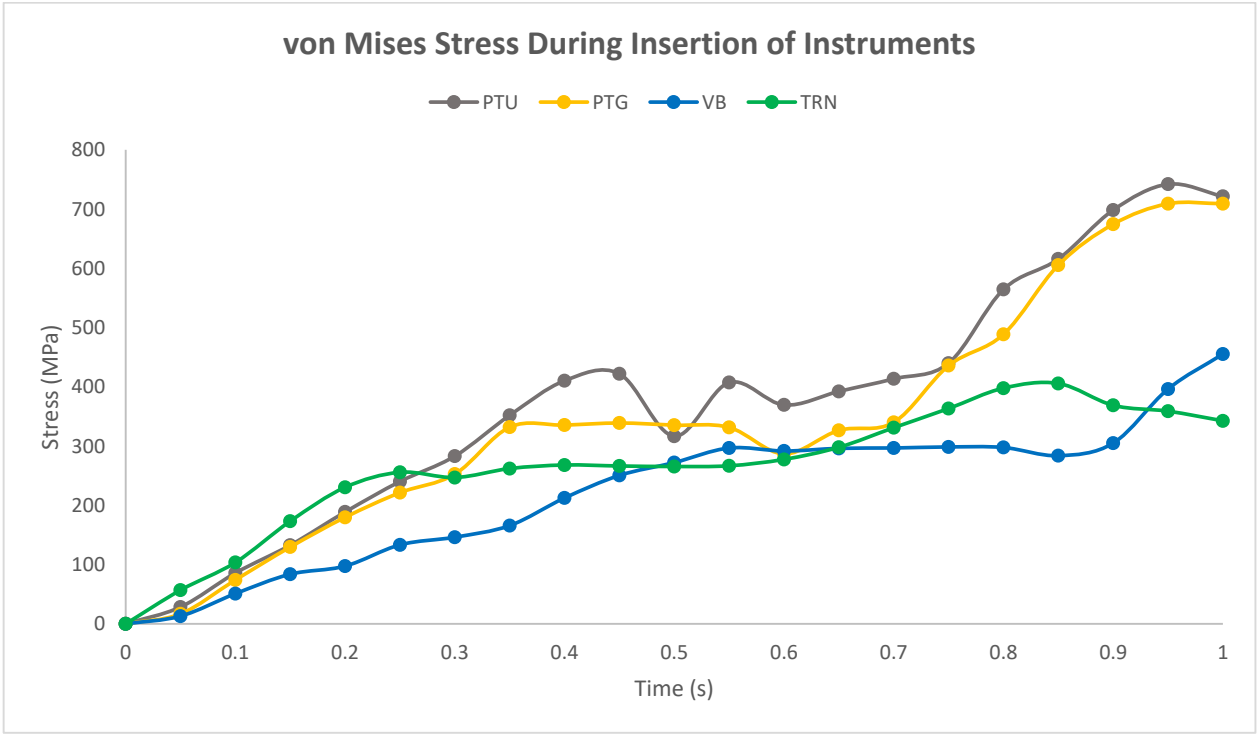

Figure 6. Comparison of von Mises stress values during insertion for PTU, PTG, VB, and TRN.

The locations of both maximum von Mises and principal stresses were identified at the end of the insertion (Table 4). To identify the distance, the query function for distance was applied to the node at the tip, the highest stress node, and then calibrated to millimeters (Figure 7).

Table 4. Comparison of experimental fragment lengths to locations of peak von Mises and maximum principal stresses.

Instrument	Experimental Fragment Length (mm)	Location of Peak von Mises Stress (mm)	Location of Maximum Principal Stress (mm)
ProTaper Universal (PTU)	5.36 ± 0.79	5.16	5.12
ProTaper Gold (PTG)	4.92 ± 1.80	5.16	4.80
Vortex Blue (VB)	3.59 ± 0.47	5.74	4.70
TruNatomy (TRN)	3.26 ± 0.47	3.60	4.38

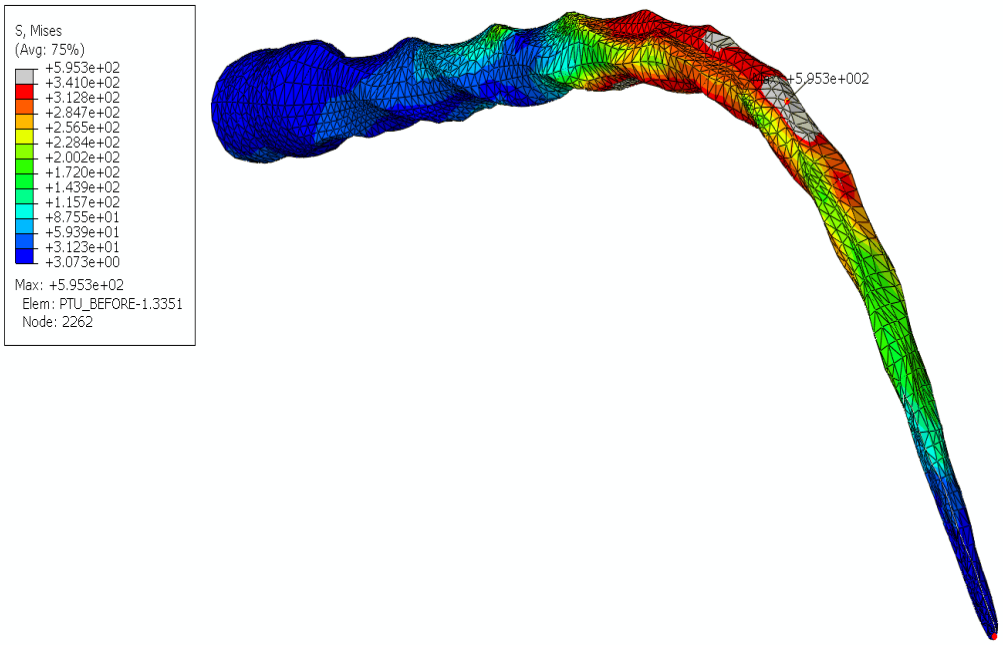

Figure 7. Location of the highest von Mises stress in VB at the end of the insertion.

In step 2, the mesh models of the instruments were allowed to rotate freely in the canal of the fatigue device. The stress values during this step did not change for all four instruments, however, the tensile-compressive actions of the instruments were observed as stress distributions alternated as the instruments rotated in the fatigue device. A cross-sectional view of the instruments at the end of the insertion was observed for both von Mises and maximum principal stress and showed stress concentrations on the outer borders of the instrument's geometry (Figure 8).

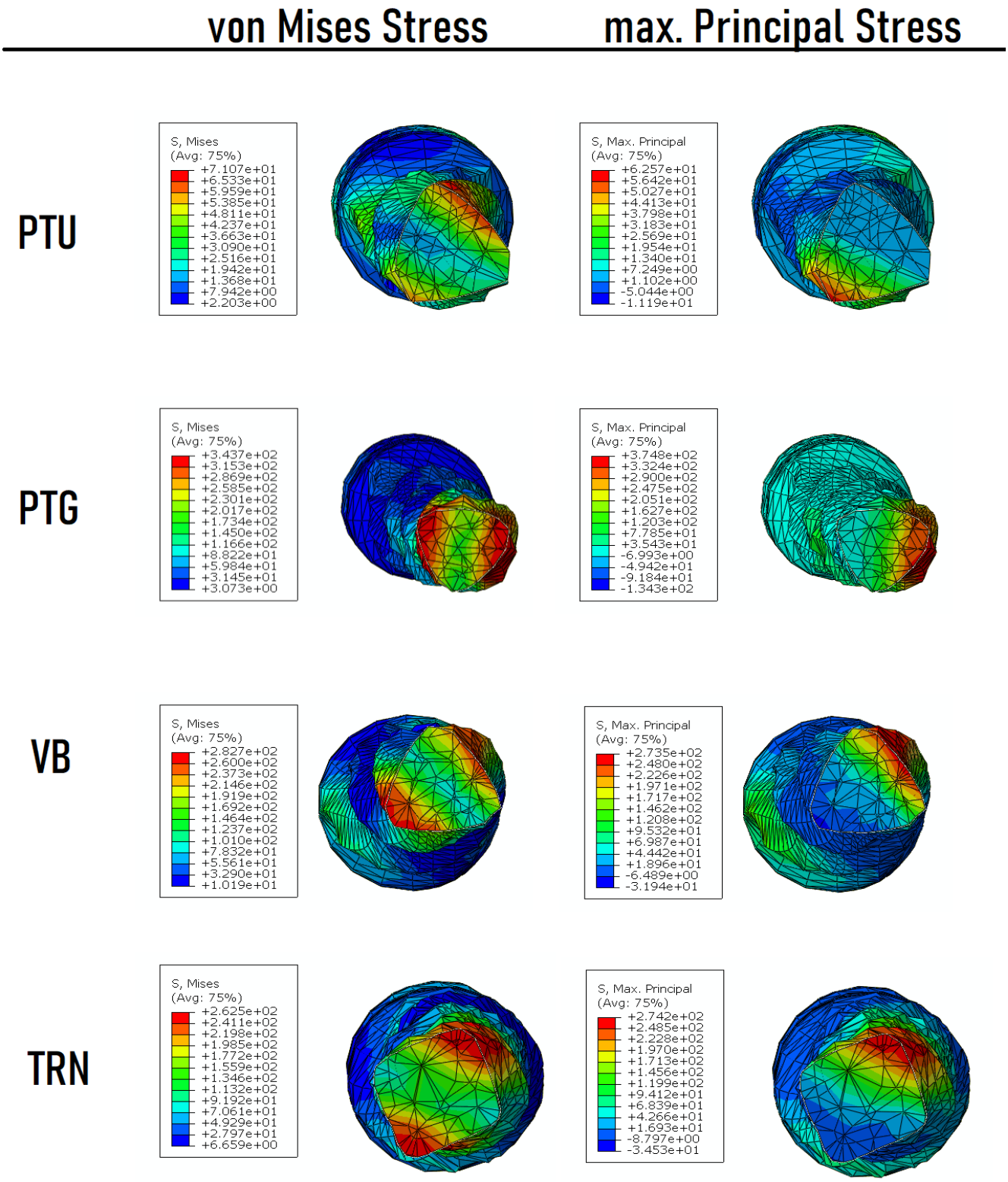

Figure 8. Stress contours viewed in the X-plane cross-section to observe differences in stress from instruments contacting the canal wall.

4. Discussion

Unlike most published endodontic literature on experimental cyclic fatigue, the present study aimed to use FEA to validate and explain experimental fatigue data rather than to compare the fatigue lives of various proprietary instrument brands. While the proposed ISO

standard is essentially a stationary fatigue test, this design has been recently criticized [3]. It should be noted that the stationary test was used for validating the finite element modeling, which in turn permits changes in experimental design, including selectable simulated instrument movements.

Owing to the intricacy and asymmetrical nature of the instrument cross-sections, micro-CT is often advantageous in situations where numerical modeling is simply too complicated to perform or too time-consuming. However, imaging methods are often limited by the resolution and artifacts generated in the scans, whereas numerical modeling assumes a perfect model. SEM imaging confirmed that the 3D models generated in InVesalius 3.1 had reasonable resemblance when considering cross-sectional and overall geometry. With respect to the mesh models, a mesh convergence test could be considered to determine the optimum mesh size.

The FEA results from the insertion and rotation processes explain the stress evolution and the fatigue failures observed in the in vitro tests. The von Mises criteria are normally applied to ductile materials, with a distortion energy failure theory used for combining multiaxial stresses (such as axial, bending, and torsional loads) into one equivalent stress, which is then compared to the yield stress of the material to judge the failure condition of the material [16,17]. Given that the von Mises stress is presented as a single, easily calculated and visualized scalar value, it is not surprising that the von Mises stress has been a standard output for most FE software packages, with the assumption that the examined material is isotropic in nature [18]. However, previous studies have reported on the anisotropic nature of NiTi, which is believed to be a result of material processing or training procedures [19–21].

Maximum principal stress is a different failure indicator; based on the concept that if a material is exposed to a multiaxial stress system, fracture will occur where the stress anywhere in the component exceeds the local strength [22]. This theorem is also limited by the assumption of isotropy in the material [18]. In FEA, there exists no perfect stress evaluation method to account for all multiaxial stresses, and it is therefore, important to note that all calculations are a simplification of experimental phenomena.

FEA verified that both the von Mises and maximum principal stresses occurred on the outer curve of the instrument (extrados). Repeated alternating stresses during cyclic rotation could lead to fatigue failure, since there were no increases in the stress distribution in the rotation step. Fractographic analysis of previous cyclic fatigue studies affirms that crack propagation begins in peripheral regions of the cross-sections, which validates the modeling of stress contours used in the present study [23–26].

Arguably, the only two instruments that are directly comparable are the PTU and the PTG, as they have identical geometries and boundary load conditions. They differ only by the absolute values of the mechanical constants in the VUMAT subroutine. During insertion, von Mises and the maximum principal stresses of the selected elements were not significantly different. PTU had the highest peak von Mises stress at 742 MPa, whereas PTG had 702 MPa. Nevertheless, this difference is unlikely to explain the large disparity in experimental NCF (PTU: 601 NCF vs. PTG: 1944 NCF).

For VB and TRN, the peak stress values recorded were significantly lower at 455 MPa and 406 MPa, respectively, which could explain the higher NCF values when compared to PTU. It is not possible to attribute this difference solely to the metallurgical properties of the instruments, as their geometries vary significantly. In the case of TRN, the taper is narrower, which could result in less contact with the canal walls, leading to a reduced stress concentration. PTU, PTG, and VB all show peak values of von Mises stress at the end of insertion, whereas TRN showed the peak stress at 0.85 s (406 MPa), but the stress values decreased as the instrument was completely inserted at 1.00 s (343 MPa).

By localizing the peak stress locations for von Mises and maximum principal stresses in the instruments, there was a good correlation with the experimental fracture locations for PTU, PTG, and TRN, with the peak stress locations falling within two standard deviations of their experimental counterparts for their fragment lengths, assuming that the peak

stresses are the region of the highest probability where crack propagation would occur. The less impressive results for VB may have been due to incorrect assumptions about some mechanical constants used for the blue-treated wire.

The rotational step did not show any changes in von Mises or maximum stresses regardless of the number of revolutions or rotational speed. Given that there are no increases in stress after a full revolution, the resulting simulation would, in effect, allow the instrument to rotate indefinitely without cyclic failure occurring. In this regard, the FE modeling was not successful in determining the fatigue life of the instruments. Hence, a failure criterion must be implemented to mimic crack propagation.

A potential way to explore crack propagation could be the extended finite element method (XFEM), where nodes that contain the crack tip are enriched with discontinuous functions provided by asymptotic nodes of displacement at the crack tip. An alternative method, as described in the study of Scattina et al., is to implement a fatigue criterion in Matlab (The Mathworks Inc., Natick, MA, USA), such as the Carptineri-Spagnoli, or 'C-S', criterion, where the study reports no relationship between experimental NCF and FEA NCF [11,27]. However, the C-S criterion is applied for high-cycle multiaxial fatigue, such as those in the order of 104 cycles, and thus, may not be a suitable criterion for endodontic instruments that have low cycle numbers [27,28]. The stress values reported in FEA could be correlated to S-N curves to predict NCF. Existing literature describes a low cyclic fatigue life for NiTi [29]. Given this, further analysis of the fatigue life of NiTi is needed, and additional factors, such as the effects of electropolishing and heat treatment, need to be accounted for.

5. Conclusions

FEA can be a useful method for recreating the stress histories of endodontic instruments in action via accurate geometrical modeling based on mechanical constants obtained from experimental data. As the stress evolution of an instrument cannot be observed experimentally, this study serves as a promising basis for the examination of the mechanical behavior of novel instruments through a standardized fatigue rig. Although the stress values and modeling were reasonable, this study was unable to replicate the NCF through FEA to give an estimated fatigue life. Further investigations into XFEM and the low-cyclic fatigue behavior of thermomechanically treated NiTi alloys could inform future instrument design.

Author Contributions: Conceptualization, P.Y.-H.C., L.J.W. and O.A.P.; methodology, P.Y.-H.C., B.W., L.J.W. and O.A.P.; software, P.Y.-H.C. and B.W.; formal analysis, P.Y.-H.C., B.W., L.J.W. and O.A.P.; investigation, P.Y.-H.C. and B.W.; data curation, P.Y.-H.C. and B.W.; writing—original draft preparation, P.Y.-H.C.; writing—review and editing, P.Y.-H.C., B.W., L.J.W. and O.A.P. All authors have read and agreed to the published version of the manuscript.

Funding: This research was funded by the Australian Dental Research Foundation (ADRF) Grant, grant No. 0072-2021 and also by the University of Queensland Research Stipend.

Institutional Review Board Statement: Not applicable.

Informed Consent Statement: Not applicable.

Data Availability Statement: The data presented in this study are openly available in: PubMed: 10.3390/ma15238367, 10.1007/s00784-021-04360-2 and Frontiers: 10.3389/fdmed.2021.744809.

Conflicts of Interest: The authors declare no conflict of interest.

References

1. Lee, M.H.; Versluis, A.; Kim, B.M.; Lee, C.J.; Hur, B.; Kim, H.C. Correlation between experimental cyclic fatigue resistance and numerical stress analysis for nickel-titanium rotary files. *J. Endod.* **2011**, *37*, 1152–1157. [CrossRef] [PubMed]
2. Pruett, J.P.; Clement, D.J.; Carnes, D.L. Cyclic fatigue testing of nickel-titanium endodontic instruments. *J. Endod.* **1997**, *23*, 77–85. [CrossRef] [PubMed]
3. Hülsmann, M.; Donnermeyer, D.; Schäfer, E. A critical appraisal of studies on cyclic fatigue resistance of engine-driven endodontic instruments. *Int. Endod. J.* **2019**, *52*, 1427–1445. [CrossRef] [PubMed]
4. Hülsmann, M. Research that matters: Studies on fatigue of rotary and reciprocating NiTi root canal instruments. *Int. Endod. J.* **2019**, *52*, 1401–1402. [CrossRef]
5. Pedullà, E.; Canova, F.S.; La Rosa, G.R.M.; Naaman, A.; Diemer, F.; Generali, L.; Nehme, W. Influence of NiTi Wire Diameter on Cyclic and Torsional Fatigue Resistance of Different Heat-Treated Endodontic Instruments. *Materials* **2022**, *15*, 6568. [CrossRef]
6. Seracchiani, M.; Reda, R.; Zanza, A.; D'Angelo, M.; Russo, P.; Luca, T. Mechanical Performance and Metallurgical Characteristics of 5 Different Single-file Reciprocating Instruments: A Comparative In Vitro and Laboratory Study. *J. Endod.* **2022**, *48*, 1073–1080. [CrossRef]
7. Peters, O.A.; Chien, P.Y.-H.; Armitt, K.; Macorra, J.C.; Arias, A. Testing cyclic fatigue resistance of nickel-titanium rotary endodontic Instruments: A validation study for a minimum quality criterion in a standardized environment. *Front. Dent. Med.* **2021**, *2*, 744809. [CrossRef]
8. Chien, P.Y.-H.; Walsh, L.J.; Peters, O.A. Finite element analysis of rotary nickel-titanium endodontic instruments: A critical review of the methodology. *Eur. J. Oral Sci.* **2021**, *129*, e12802. [CrossRef]
9. Liu, G.R.; Quek, S.S.; Liu, G.R. *Finite Element Method*; Elsevier Science & Technology: Oxford, UK, 2003.
10. Margetts, L.; Smith, I.M.; Griffiths, D.V.; Margetts, L.; Griffiths, D.V. *Programming the Finite Element Method*, 5th ed.; Smith, I.M., Griffiths, D.V., Margetts, L., Eds.; John Wiley & Sons Inc.: Chichester, UK, 2014.
11. Scattina, A.; Alovisi, M.; Paolino, D.S.; Pasqualini, D.; Scotti, N.; Chiandussi, G.; Berutti, E. Prediction of Cyclic Fatigue Life of Nickel-Titanium Rotary Files by Virtual Modeling and Finite Elements Analysis. *J. Endod.* **2015**, *41*, 1867–1870. [CrossRef]
12. Chien, P. Cyclic Fatigue Resistance of Nickel-Titanium Rotary Endodontic Instruments: An Experimental and Finite Element Analysis Study. Master's Thesis, The University of Queensland, St. Lucia, Australia, 2022.
13. Chien, P.Y.-H.; Martins, J.N.R.; Walsh, L.J.; Peters, O.A. Mechanical and metallurgical characterization of Nickel-Titanium wire types for rotary endodontic instrument manufacture. *Materials* **2022**, *15*, 8367. [CrossRef]
14. Martins, S.C.S.; Silva, J.D.; Garcia, P.R.; Viana, A.C.D.; Buono, V.T.L.; Santos, L.A. Influence of cyclic loading in NiTi austenitic and R-phase endodontic files from a finite element perspective. *Clin. Oral Investig.* **2022**, *26*, 3939–3947. [CrossRef] [PubMed]
15. van der Vyver, P.J.; Vorster, M.; Peters, O.A. Minimally invasive endodontics using a new single-file rotary system. *Int. Dent. Afr. Ed.* **2019**, *9*, 6–20.
16. Bai, Q.; Bai, Y. Chapter 9—Thermal expansion design. In *Subsea Pipeline Design, Analysis, and Installation*; Bai, Q., Bai, Y., Eds.; Gulf Professional Publishing: Boston, MA, USA, 2014; pp. 187–220.
17. Budynas, R.; Nisbett, J.K. *Shigley's Mechanical Engineering Design*; McGraw-Hill US Higher Ed USE: New York, NY, USA, 2018.
18. Korenczuk, C.E.; Votava, L.E.; Dhume, R.Y.; Kizilski, S.B.; Brown, G.E.; Narain, R.; Barocas, V.H. Isotropic failure criteria are not appropriate for anisotropic fibrous biological tissues. *J. Biomech. Eng.* **2017**, *139*, 0710081–07100810. [CrossRef] [PubMed]
19. Mehrabi, R.; Andani, M.T.; Elahinia, M.; Kadkhodaei, M. Anisotropic behavior of superelastic NiTi shape memory alloys; an experimental investigation and constitutive modeling. *Mech. Mater.* **2014**, *77*, 110–124. [CrossRef]
20. Zheng, Q.S.; Liu, Y. Prediction of the detwinning anisotropy in textured NiTi shape memory alloy. *Philos. Mag. A* **2002**, *82*, 665–683. [CrossRef]
21. Sedlák, P.; Frost, M.; Benešová, B.; Zineb, T.B.; Šittner, P. Thermomechanical model for NiTi-based shape memory alloys including R-phase and material anisotropy under multi-axial loadings. *Int. J. Plast.* **2012**, *39*, 132–151. [CrossRef]
22. Todinov, M.T. Chapter 16—Locally initiated failure and risk reduction. In *Risk-Based Reliability Analysis and Generic Principles for Risk Reduction*; Todinov, M.T., Ed.; Elsevier: Oxford, UK, 2007; pp. 315–345.
23. Mecholsky, J.; Barrett, A.; Jones, C.; Pace, K.; Nair, U. Fractographic analysis of separated endodontic file designs. *J. Mater. Sci. Mater. Med.* **2020**, *31*, 104. [CrossRef]
24. Cheung, G.S.P.; Peng, B.; Bian, Z.; Shen, Y.; Darvell, B.W. Defects in ProTaper S1 instruments after clinical use: Fractographic examination. *Int. Endod. J.* **2005**, *38*, 802–809. [CrossRef]
25. Shen, Y.; Cheung, G.S.P.; Peng, B.; Haapasalo, M. Defects in nickel-titanium instruments after clinical use. Part 2: Fractographic analysis of fractured surface in a cohort study. *J. Endod.* **2009**, *35*, 133–136. [CrossRef] [PubMed]
26. Azimi, S.; Delvari, P.; Hajarian, H.C.; Saghiri, M.A.; Karamifar, K.; Lotfi, M. Cyclic fatigue resistance and fractographic analysis of race and Protaper rotary NiTi instruments. *Iran. Endod. J.* **2011**, *6*, 80–86. [PubMed]
27. Carpinteri, A.; Spagnoli, A.; Vantadori, S.; Bagni, C. Structural integrity assessment of metallic components under multiaxial fatigue: The C–S criterion and its evolution. *Fatigue Fract. Eng. Mater. Struct.* **2013**, *36*, 870–883. [CrossRef]

28. Murakami, Y.; Miller, K.J. What is fatigue damage? A view point from the observation of low cycle fatigue process. *Int. J. Fatigue* **2005**, *27*, 991–1005. [CrossRef]
29. Figueiredo, A.M.; Modenesi, P.; Buono, V. Low-cycle fatigue life of superelastic NiTi wires. *Int. J. Fatigue* **2009**, *31*, 751–758. [CrossRef]